


Identification of a conserved subset of cold tumors responsive to immune checkpoint blockade

Jade Moore,¹ Jim Gkantalas,¹ Ines Guix,¹ William Chou,¹ Kobe Yuen,² Ann A Lazar,³ Matthew Spitzer,⁴ Alexis Combes,⁵ Mary Helen Barcellos-Hoff ¹

To cite: Moore J, Gkantalas J, Guix I, *et al.* Identification of a conserved subset of cold tumors responsive to immune checkpoint blockade. *Journal for ImmunoTherapy of Cancer* 2025;13:e010528. doi:10.1136/jitc-2024-010528

► Additional supplemental material is published online only. To view, please visit the journal online (<https://doi.org/10.1136/jitc-2024-010528>).

Accepted 03 February 2025

ABSTRACT

Background The efficacy of immune checkpoint blockade (ICB) depends on restoring immune recognition of cancer cells that have evaded immune surveillance. Transforming growth factor-beta (TGFβ) is associated with immune-poor, so-called cold tumors whereas loss of its signaling promotes DNA misrepair that could stimulate immune response.

Methods We analyzed transcriptomic data from IMvigor210, The Cancer Genome Atlas, and Tumor Immune Syngeneic MOuse data sets to evaluate the predictive value of high βAlt, a score representing low expression of a signature consisting of TGFβ targets and high expression of genes involved in error-prone DNA repair. The immune context of βAlt was assessed by evaluating tumor-educated immune signatures. An ICB-resistant, high βAlt preclinical tumor model was treated with a TGFβ inhibitor, radiation, and/or ICB and assessed for immune composition and tumor control.

Results We found that a high βAlt score predicts ICB response yet is paradoxically associated with an immune-poor tumor microenvironment in both human and mouse tumors. We postulated that high βAlt cancers consist of cancer cells in which loss of TGFβ signaling generates a TGFβ rich, immunosuppressive tumor microenvironment. Accordingly, preclinical modeling showed that TGFβ inhibition followed by radiotherapy could convert an immune-poor, high βAlt tumor to an immune-rich, ICB-responsive tumor. Mechanistically, TGFβ inhibition increased activated natural killer (NK) cells, which were required to recruit lymphocytes to respond to ICB in irradiated tumors. NK cell activation signatures were also increased in high βAlt, cold mouse and human tumors that responded to ICB.

Conclusions These studies indicate that loss of TGFβ signaling competency and gain of error-prone DNA repair identifies a subset of cold tumors that are responsive to ICB. Our mechanistic studies show that inhibiting TGFβ activity can convert a high βAlt, cold tumor into ICB-responsive tumors via NK cells. A biomarker consisting of combined TGFβ, DNA repair, and immune context signatures is a means to prospectively identify patients whose cancers may be converted from cold to hot with appropriate therapy.

WHAT IS ALREADY KNOWN ON THIS TOPIC

⇒ For some patients with cancers infiltrated with lymphocytes, response to immune checkpoint blockade (ICB) provides durable tumor control. However, an ICB response for patients whose tumors lack lymphocytic infiltration is considered unlikely.

WHAT THIS STUDY ADDS

⇒ The βAlt score, which reports a DNA repair deficiency caused by loss of transforming growth factor-beta (TGFβ) signaling, predicts response to ICB in clinical trial data from IMvigor210 patients with metastatic bladder cancer and for patients with melanoma. Notably, transcriptomic assessment of the immune context shows that these are immune-poor, so-called cold tumors. Preclinical modeling indicates that alleviating TGFβ inhibition of natural killer cells is critical to restoring immune recognition.

HOW THIS STUDY MIGHT AFFECT RESEARCH, PRACTICE OR POLICY

⇒ Our work identifies a highly conserved tumor phenotype consisting of cancer cells that have lost TGFβ signaling and gained error-prone DNA repair embedded in a TGFβ rich, immune-poor microenvironment. A high βAlt, immune poor mouse tumor could be converted to ICB responsive following treatment with radiation and TGFβ inhibitors. Hence, the βAlt score provide the means to prospectively identify a previously unrecognized subset of immune poor patients in whom TGFβ inhibition reverses resistance to ICB.



© Author(s) (or their employer(s)) 2025. Re-use permitted under CC BY-NC. No commercial re-use. See rights and permissions. Published by BMJ Group.

For numbered affiliations see end of article.

Correspondence to

Dr Mary Helen Barcellos-Hoff; MaryHelen.Barcellos-Hoff@ucsf.edu

BACKGROUND

Understanding the specific mechanisms by which cancer has subjugated the immune system is essential for cancer immunotherapy to restore immune recognition. The canonical example is immune checkpoint blockade (ICB) targeting programmed cell death protein 1 or programmed death-ligand 1 (PD-1/PD-L1) or cytotoxic T-associated lymphocyte 4, which are now the standard of care for many adult cancers, yielding significant and durable clinical responses in a subset of patients.¹ Patient selection for ICB is

primarily guided by histopathological assessment of PD-L1 expression and/or the spatial distribution or density of tumor-infiltrating lymphocytes.² High tumor mutation burden (TMB) is also associated with response to ICB in several settings^{3,4} and is a Food and Drug Administration-approved biomarker for ICB in certain cancers.^{5,6} Experimentally, cancers are frequently characterized in terms of immune composition, as immune-rich, “hot” or infiltrated versus immune deserts, “cold”, or devoid of lymphocytes.^{7–10} Various methods, including digital pathology, transcriptional signatures, and immunohistochemistry, report lymphocytic infiltration.^{11,12} Patients with tumors infiltrated with lymphocytes are considered good candidates for ICB response, whereas those whose tumors lack lymphocytes are not.

A notable success for predicting patient response stemmed from the recognition that patients with mismatch repair deficient (dMMR) tumors were enriched in some early ICB trials.¹³ This led to the NICHE-2 trial in which most patients with colorectal cancer with dMMR responded to neoadjuvant ICB therapy; moreover, the association of dMMR with response rate and duration to ICB is also predictive in 12 other tumor types.¹⁴ Mismatch repair of intrinsic or extrinsic DNA damage in the dMMR context is believed to provoke immune recognition through increased neoantigen production, release, and presentation.^{15,16} Consistent with this, dMMR tumors are highly inflamed due to cytosolic DNA sensing mediated by cyclic GMP–AMP synthase (cGAS)—stimulator of interferon genes (STING) pathway that elicits type I interferon (IFN) signaling to provoke lymphocyte recruitment.¹⁷

Transforming growth factor-beta (TGF β) is a high-value target in cancer therapy because it promotes a permissive tumor microenvironment (TME) and invasive cancer phenotypes while suppressing antitumor immunity.^{18,19} Notably, TGF β also has a crucial role in regulating the DNA damage response.²⁰ TGF β positively regulates canonical DNA repair by homologous recombination and non-homologous end-joining and suppresses repair by error-prone alternative end-joining (alt-EJ).^{20–22} This relationship is reported by gene signatures consisting of TGF β signaling targets and genes necessary for alt-EJ DNA repair, which are significantly anticorrelated across most tumor types and represented by a score termed β Alt that predicts response to genotoxic therapy.^{23,24} Cancers with a high β Alt score are those in which expression of TGF β target genes are low, indicating that signaling is compromised, and express high levels of alt-EJ genes, indicating poor DNA repair. Consistent with defective DNA repair, high β Alt tumors have a greater fraction of the genome altered, are characterized by a specific indel mutation, and are more responsive to chemoradiation.²³

Since genomic instability is a hallmark of cancer and can induce type I IFN to activate innate immunity,²⁵ it has been proposed that specific DNA repair deficiencies associated with response to genotoxic therapies may also predict response to immunotherapy.²⁶ Given that TGF β determines DNA repair competency, we hypothesized

that low β Alt tumors, exhibiting high expression of TGF β target genes, have obligate TGF β activity and would be immune-poor. In contrast, high β Alt cancers with impaired TGF β signaling resulting in poor DNA repair, like those with dMMR, would be infiltrated ICB and hence predict response. We tested this hypothesis by determining both β Alt scores and the immune context for tumors of patients who responded to immunotherapy in clinical trials. High β Alt strongly correlated with ICB response in patients with both bladder cancer and melanoma but was unexpectedly associated with immune-poor cancers. Indeed, the association between high β Alt and immune-poor cancers was highly conserved across human cancer types and in mouse cancers. Mechanistic studies in preclinical models showed that TGF β blockade in irradiated tumors activated natural killer (NK) cells that were required to recruit lymphocytes and respond to ICB. Consistent with this, NK cell activation was also evident in immune-poor human tumors that responded to ICB.

These studies identified a previously unrecognized subset of immune-poor, cold tumors whose β Alt status predicts ICB response.

METHODS

Animals

All animal experiments were performed at the University of California, San Francisco (UCSF, San Francisco, California, USA). The protocols for animal husbandry and experiments were conducted with approval from the UCSF institutional review board (AN142057-01A) and adhered to the National Institutes of Health Guide for the Care and Use of Laboratory Animals. Eight-week-old B6BL/cJ *Mus musculus* (RRID: IMSR_JAX:000651) from Jackson Laboratory (Sacramento, California, USA) were purchased and housed five per cage, fed Lab Diet #5001 Rodent Formulation (Purina Animal Nutrition), and supplied water ad libitum.

Mammary tumor-derived transplants

For the treatment experiments, 8–10-week-old mice were transplanted orthotopically with F2 mammary tumor-derived transplants (mTDT) from family F previously described.²⁷ For all experiments, mice were palpated three times a week until the tumor reached 2×2, and then daily on randomization into treatment groups when the tumor reached 65–100 mm³. Tumor burden was calculated based on $0.52 \times w \times l^2$ and used to randomize mice to treatment groups as follows: Sham immunoglobulin G (IgG), anti-PD-L1, TGF β inhibition (TGF β i) with small molecule IPW or single-dose radiation (RT) treatment, and dual and triple combinations.

All agents were administered intraperitoneally (i.p.) 24 hours before irradiation at the indicated schedule for up to 3 weeks. Anti-PD-L1 (Roche) was administered once a week (10 mg/kg, PD-L1 9708, 6E11), TGF β small molecule inhibitor IPW-5371 (Innovation Pathways;

designated as IPW) was administered daily (20 mg/kg), or IgG control antibody (Bio X Cell BP0083) three times per week (25 mg/kg). Tumors were irradiated with 10 Gy using a small animal radiation research platform (SARRP, XStrahl) and individualized plans (Muriplan, XStrahl) based on arc beam CT. For in vivo depletion of NK cells, mice received 50 µg i.p. of asialo-GM1 polyclonal antibody (eBioscience, RRID: AB_10718540) 2 days before and 1 day after irradiation.

Mice were monitored daily and sacrificed for tumor ulcers or weight loss greater than 15% of body weight in accordance with the UCSF Institutional Animal Care and Use Committee (IACUC) guidelines. Technicians blinded to treatment performed tumor measurements and tissue collection. Each mouse was assigned to one of two categories based on tumor growth during the first 7 days post-treatment: responders (R) and non-responders (NR). Mice whose tumor volumes did not double from the start of treatment until 7 days post-treatment were classified as responders, whereas mice whose tumors doubled or more were classified as non-responders. Sham-irradiated, IgG-treated (control) mice were excluded from therapeutic response estimation.

RNA sequencing

For bulk RNA sequencing, fragments (~50 mg) of liquid nitrogen-preserved mTDT were shipped on dry ice to Q² Solutions | EA Genomics to isolate total RNA using proprietary methods. The quantity and quality of the specimens were assessed using an Agilent Bioanalyzer and NanoDrop analysis. Total RNA samples that met the quality control metrics were enriched for messenger RNA (mRNA), fragmented, and converted into indexed complementary DNA (cDNA) libraries for Illumina sequencing. The generated cDNA libraries were quantified by quantitative PCR using primers specific for Illumina sequencing adapters, and TruSeq Stranded mRNA in a 30 M 50bp paired-end assay. Raw sequencing data were obtained in FASTQ format. Read mapping was performed using the Rsubread package (RRID: SCR_016945) against *Mus musculus* GRCm38 and the human GRCh38 genome (28). Gene expression data archived in the Gene Expression Omnibus (GEO, RRID: SCR_005012) are pending.

Multispectral flow cytometry

Tumor and blood cells from mice treated as described were counted with 1:1 Trypan blue/cells and blocked with 0.25 mg TruStain FcX PLUS antibody (BioLegend Cat#156603, clone S17011E) per 10⁶ cells in 0.1 mL cell staining buffer (CSB, 0.5% fetal bovine serum in phosphate-buffered saline (PBS)) for 30 min on ice. Cells were then washed with PBS and incubated with LIVE/DEAD Zombie Aqua (1:2000, BioLegend Cat#423101) in 0.02 mL PBS and subsequently stained in 0.08 mL CSB using a panel of optimized fluorophore-conjugated cell surface antibodies (online supplemental table 1) for 1 hour at 4°C in the dark. Cells were then washed 1× with 2 mL CSB, followed by centrifugation at 350×g for

5 min at 4°C. The supernatant was aspirated, and the cell pellet was in 0.5 mL/tube FluoroFix buffer (BioLegend Cat#422101) in the dark for 1 hour at room temperature for fixation. For intracellular staining, the nucleus was washed and permeabilized by resuspending in 0.5 mL 1× intracellular staining permeabilization wash buffer (BioLegend Cat#421002) diluted in distilled water, centrifuged at 350×g for 5 min at 4°C, and incubated with fluorophore-conjugated intracellular antibodies for 30 min in the dark at room temperature. Cells were then washed 2× with 2 mL intracellular staining perm wash buffer and centrifuged at 350×g for 5 min at 4°C before resuspending the cells in CSB (0.5 mL) and analyzed on a 3-laser Cytek Northern Lights spectral cytometer (Fremont, California, USA). The experimental samples were unmixed using appropriate cell-based single-color controls in SpectroFlo (Cytek Biosciences). Data analysis was performed using the Flow Cytometry Software (FCS) Express 7 Research Edition De Novo software (Pasadena, California, USA), employing suitable gating strategies (online supplemental table 2) for each tissue. Each surface marker was expressed as median fluorescence intensity. An unsupervised analysis was performed using the dimensionality reduction algorithm t-distributed stochastic neighbor embedding (t-SNE) with the Barnes-Hut approximation to identify and visualize populations. All FCS files were merged, and 100,000 live CD45+ cells were randomly downsampled from each sample to be subjected to the transformation algorithm to form clusters according to the expression levels of cell-surface phenotyping markers. Samples were grouped and overlaid according to treatment and response to visualize the differences in immune cell composition.

Bioinformatics analyses

Gene expression heatmaps were constructed by hierarchical clustering using the R package ComplexHeatmap.²⁸ Gene expression values were normalized z-scores for all heatmaps; Euclidian distance and ward.D.2 clustering was used.

βAlt scores for preclinical tumors or patients were calculated based on the expression pattern using the previously published TGFβ and alt-EJ gene signatures,²³ weighted as described.²⁴ The composition of each signature is listed in online supplemental table 3. In brief, the weight of each TGFβ gene and each alt-EJ gene was calculated by multiplying by its factor, and the βAlt weighted score was calculated as the sum of the weighted expression of the genes from each signature for each tumor. This βAlt score conveys the relative expression of each signature for each tumor.

Previously reported tumor-educated immune signatures (TeIS) gene signatures²⁹ are listed in online supplemental table 4. The feature gene signature scores for the 10 cell types included T cell, myeloid, CD90+CD44+ stroma, CD4, CD8, T regulatory cells, macrophages, monocytes, classical dendritic cell (cDC)1, and cDC2.²⁹

Data sets

The Cancer Genome Atlas (TCGA) data set was downloaded from the Genomic Data Commons portal from the EBPlusPlusAdjustPANCAN_IlluminaHiSeq_RNASeqV2.geneExp.tsv file. The downloaded gene expression values were trimmed as the mean of M values normalized, log2 transformed, and mean-centered per gene by converting them into z-scores. Primary solid tumor samples were analyzed. TCGA somatic mutations at the individual level were obtained following approval from the dbGaP Data Access Committee (Project #11689).³⁰

The source code and processed data for IMvigor210 trial (NCT02108652) were accessed in IMvigor210CoreBiologies, a fully documented software, and package for the R statistical computing environment.¹⁰ The IMvigor210 data set was from the European Genome-Phenome Archive under accession number EGAS00001004997.³¹ The GSE78220 melanoma data set (n=28 specimens)³² and GSE91061 melanoma data set (n=109 specimens with 58 on-treatment and 51 pretreatment) from 65 patients³³ were downloaded from the GEO (RRID: SCR_005012) in January 2022 using the R package GEOquery. In GSE78220, samples were pair-end sequenced with a read length of 2×100 bp (Illumina HiSeq2000) and amplified to the UCSC hg19 reference genome using Tophat2³⁴ and normalized expression levels of genes were expressed in fragments per kilobase of transcript per million mapped reads (FPKM) values as generated by cuffquant and cuffnorm.³⁵ In GSE91061, raw FASTQ files were aligned to the hg19 genome using the STAR aligner (STAR, RRID: SCR_004463), counted, and annotated using Rsamtools V.3.2, and the TxDb.Hsapiens.UCSC.hg19.known gene transcript database. Raw reads were normalized using a regularized logarithm transformation function with a robust estimation. The Tumor Immune Syngeneic Mause (TISMO) database was similarly accessed.³⁶

Statistical analysis

Descriptive statistics were used to summarize the data. Frequencies and counts were used to describe categorical variables, whereas mean, SD, median, and interquartile range (IQR) were used for numeric data. X² or Fisher's exact test, as appropriate, was used to compare categorical variables, and the Mann-Whitney test was used for numeric variables. Overall survival was defined as the time from the start of randomization of treatment assignment to the date of sacrifice, as directed by the IACUC guidelines. Hazard ratio (HR) and associated 95% confidence interval (CI) were computed using multivariate Cox regression analyses. Proportional hazards were evaluated using the interaction between the log of time and each variable; we found no statistical evidence to indicate proportional hazard violation, given that the p value was >0.05. Two-sided p values less than 0.05 were considered statistically significant. All experimental data was analyzed using Prism 7 (GraphPad Prism, RRID: SCR_002798) and SAS V.9.4.

RESULTS

High β Alt correlates with ICB response

To test the hypothesis that β Alt would predict response to ICB, we used the IMvigor210 trial data set in which patients with metastatic bladder cancer were treated with anti-PD-L1 (atezolizumab) and platinum chemotherapy.^{10 31} Patients were classified according to response evaluation criteria in solid tumors (RECIST) as responders, which encompassed complete response and partial response, and as non-responders if the disease remained stable or progressed. β Alt was assessed by dimensionally collapsing the correlation of a chronic TGF β signature consisting of 50 TGF β target genes and a signature composed of 36 alt-EJ repair genes that TGF β suppresses^{23 24} (online supplemental table 3). A high β Alt score represents cancers in which TGF β signaling is low and error-prone DNA repair is high.

As previously reported for TCGA and other data sets, the anticorrelation between the expression of these signatures, indicative of their functional relationship in which TGF β suppresses alt-EJ gene expression, was recapitulated in unsupervised clustering of IMvigor 210 RNA-seq data (n=348) (figure 1A). Single-specimen gene set enrichment (ssGSEA) of each signature were also significantly anticorrelated (Pearson correlation coefficient $r=-0.48$, $p<0.0001$; figure 1B). Next, we plotted the β Alt scores as a function of ICB response. The mean β Alt was significantly ($p<0.0001$) larger in responders (R, n=68, $\bar{x}=17.5$) than non-responders (NR, n=230; $\bar{x}= -10.1$; figure 1C). To validate this finding, we analyzed the GSE78220 data set reported by Hugo *et al* from patients with metastatic melanoma treated with anti-PD-1 (pembrolizumab), in which 15 of 27 (55%) patients were classified as responders.³² As with IMvigor210, the β Alt scores of responders were significantly greater ($p<0.05$, Mann-Whitney test, 95% CI (-0.42 to -63.0)) compared with those whose disease progressed (online supplemental figure S1A).

Patients whose tumors fell in the high β Alt quartile (Q4) had a median survival of 10.9 months and experienced better overall survival (HR 0.62, $p=0.011$) compared with those ranked as low β Alt (Q1), whose median survival was 8.1 months (figure 1D). The fraction of patients who were responders was significantly enriched in Q4 versus Q1 ($p=0.0031$; figure 1E). Indeed, two-thirds of the IMvigor210 responders had β Alt scores above 0 (45/68, 66%). IMvigor210 comprised two cohorts of patients: cohort 1 was platinum ineligible and treatment naïve at the time of immunotherapy, cohort 2 had failed prior treatment with platinum chemotherapy.^{37 38} Notably, the frequency of complete and partial response by RECIST criteria was significantly greater for those ranked as high β Alt (Q4) compared with those ranked who ranked low (Q1) in both Cohort 1 ($p=0.0045$) and Cohort 2 ($p=0.023$; online supplemental figure S1B).

Mariathasan *et al*¹⁰ reported that patient response was significantly associated with TMB. As expected from error-prone DNA repair, the β Alt score is associated with the fraction of genome altered.²³ β Alt is also significantly

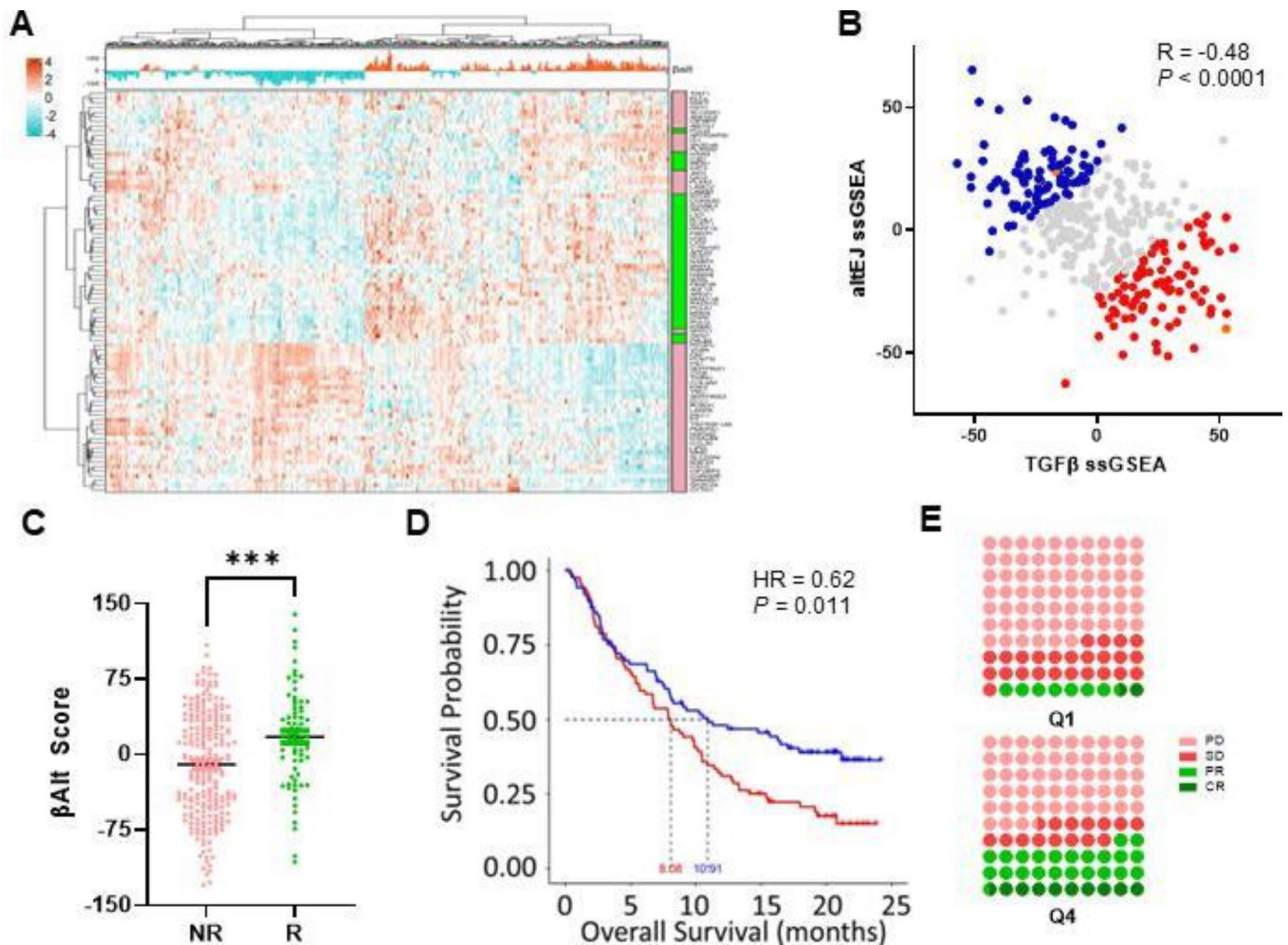


Figure 1 High β Alt is associated with ICB response. Analysis of data from IMvigor210 patient with metastatic bladder (n=348). (A) Unsupervised hierarchical clustering heatmap depicting TGF β (pink) and alt-EJ (green) gene signatures of patients (n=348). β Alt score is annotated above (coral=high, teal=low). (B) TGF β and alt-EJ ssGSEA scores are negatively correlated (R=-0.48, p<0.0001). The high quartile (Q4; n=87, blue) and low quartile (Q1, n=87, red) are indicated. (C) The IMvigor210 patients defined as responders (R, n=68) have significantly higher mean β Alt score of (\bar{x} = 17.5 \pm 6.1 SEM) versus those designated non-responders (NR, n=230; \bar{x} = -10.1 \pm 3.4 SEM), p<0.0001, Wilcoxon test. (D) Overall survival of patients in high (Q4, blue) versus low (Q1, red) β Alt quartiles designated in 1B. Kaplan-Meier analysis, HR=0.62, p=0.011 calculated via log-rank test. (E) Distribution of response types (complete response, CR; partial response, PR; progressive disease, PD; stable disease, SD) for β Alt Q1 (n=79) and Q4 (n=75). Q4 is significantly enriched for CR and PR. p=0.0031, χ^2 test. alt-EJ, alternative end-joining; ICB, immune checkpoint blockade; ssGSEA, single-specimen gene set enrichment analysis; TGF β , transforming growth factor-beta.

correlated with TMB, as well as predicted neoantigen frequency, in IMvigor210 (online supplemental figure S1C,D). Mariathasan *et al* also reported that a TGF β expression signature is associated with the immune excluded pattern of lymphocyte distribution. Mapping Mariathasan *et al* assignment of immune infiltrate annotated for prior chemotherapy, response, β Alt score, and TMB revealed that high β Alt scores were distributed broadly, i.e., not associated with a particular pattern of lymphocyte distribution (online supplemental figure S1E).

The significant association of β Alt with response to ICB in two patient populations substantiates the predictive value of high β Alt for ICB, and also reports sensitivity to genotoxic treatments due to poor DNA repair.^{23 24}

High β Alt correlates with the immune composition in a tissue-agnostic manner

Next, we investigated the specific immune context based on the expectation that high β Alt, like dMMR tumors,¹⁷ would be infiltrated. The challenges of classifying the frequency and pattern of tumor-infiltrating lymphocytes and immune composition objectively and reproducibly have prompted several approaches.³⁹ Here, we used 10 TeIS (online supplemental table 4) defined by immune profiling immune cells isolated from 364 surgical tumor specimens across 12 tissues.²⁹ We conducted unsupervised clustering of TeIS expression for IMvigor210 specimens that resulted in an expression gradient from immune-rich to immune-poor (figure 2A). Annotation of this heatmap for β Alt showed a broad parallel transition from

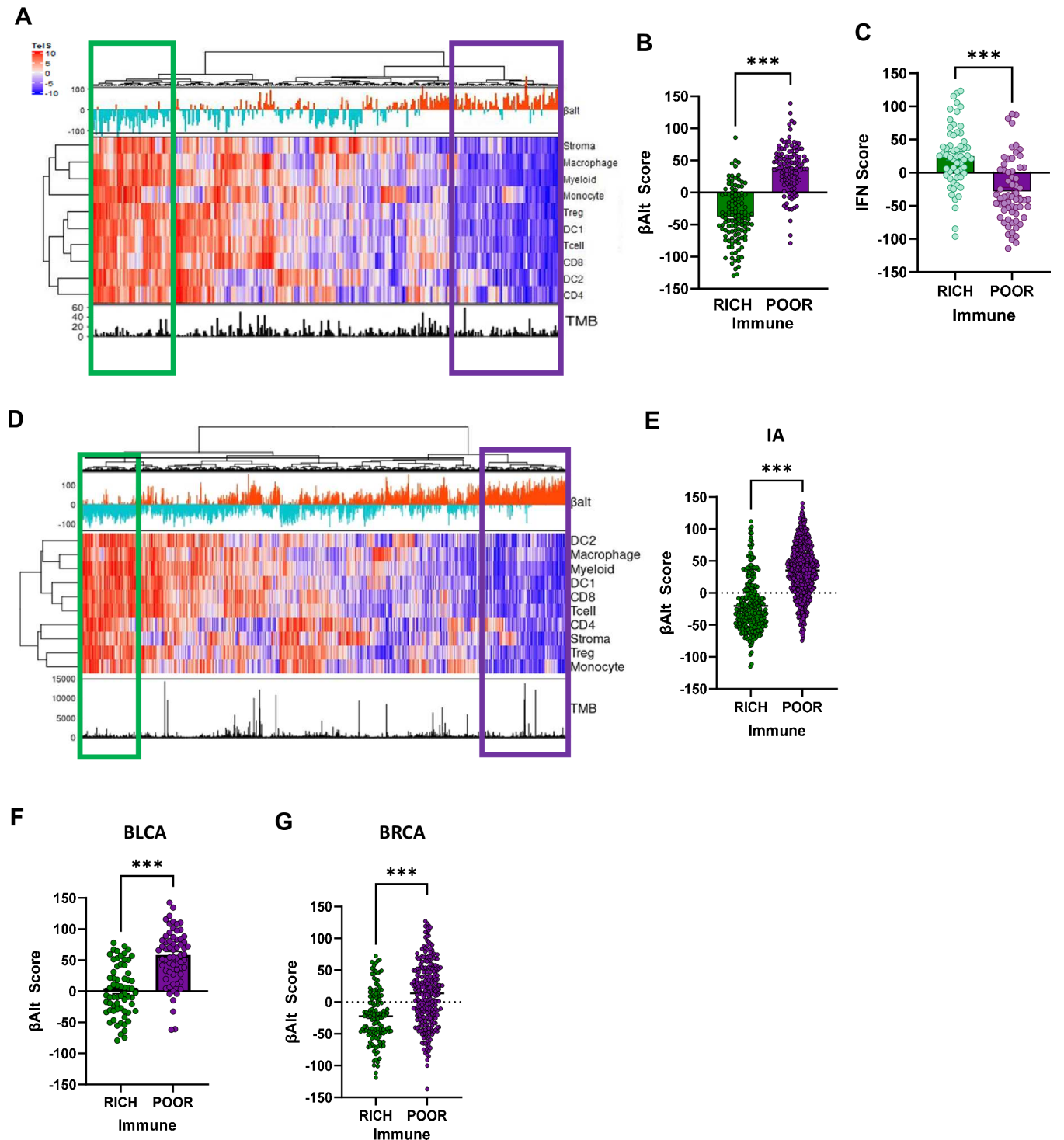


Figure 2 High β Alt correlates with the immune composition in a tissue-agnostic manner. (A) Unsupervised clustering of TelS heatmap IMvigor210 patient with metastatic bladder (n=348) annotated for β Alt score above and tumor mutation burden (TMB) below. The green box designates an immune-rich cluster (n=116); the purple box designates an immune-poor cluster (n=116). (B) β Alt scores of IMvigor210 tumors classified as immune-rich are significantly lower than those designated as immune-poor ($p < 0.001$; Wilcoxon test). (C) IFN signature scores of IMvigor210 immune-poor tumors are significantly lower than immune-rich tumors. ($p < 0.001$; Wilcoxon test). (D) Unsupervised hierarchical clustering of TelS signatures for immune archetype TCGA data set (n=4341) from Combes *et al* 2021 annotated with β Alt scores (red=positive, teal=negative) above and tumor mutation burden (TMB) below. The immune-rich cluster is designated by a green box, the immune-poor cluster is designated by a purple box. (E–F) β Alt score distribution of immune-rich (green) versus immune-poor (purple) clusters for: (E) TCGA IA data set from Combes *et al*; immune-rich (n=297) and immune-poor (n=523). Wilcoxon test. (F) TCGA bladder cancer (BLCA; immune-rich, n=65; immune-poor, n=67). Unpaired t-test. (G) TCGA breast cancer (BRCA; immune-rich, n=135 and immune-poor, n=267). Unpaired t-test. Statistical significance is denoted as ** $p < 0.01$, *** $p < 0.001$. IFN, interferon; TCGA, The Cancer Genome Atlas; TelS, tumor-educated immune signature.

immune-rich, low β Alt to immune-poor, high β Alt. Separating the cluster with the highest and the lowest mean TeIS expression confirmed that immune-poor tumors had significantly higher β Alt scores when compared with immune-rich tumors ($p < 0.001$, [figure 2B](#)). Of the IMvigor210 responders with high β Alt scores (31/68), 74% were classified as immune-poor (23/31). Consistent with a cold phenotype, the immune-poor group had significantly lower expression of a type I IFN gene signature⁴⁰ ([figure 2C](#), online supplemental figure S2A). Assessing TeIS as a function of lymphocytic distribution assigned in Mariathasan *et al*, showed that desert tumors were enriched for immune-poor TeIS signatures, inflamed tumors were predominantly immune-rich, and excluded tumors exhibit a range of TeIS scores (online supplemental figure S2B).

The unexpected characterization of high β Alt as immune-poor tumors led us to test the association of β Alt across a subset of TCGA solid tumors ($n = 4,341$) that had been assigned immune archetypes.²⁹ Unsupervised clustering of TeIS replicated the parallel transition of low-to-high β Alt with immune-rich to immune-poor ([figure 2D](#)) observed in IMvigor210 bladder cancer. Likewise, immune-poor cancers had the highest β Alt scores ([figure 2E](#)). We then examined the entire TCGA bladder cancer cohort, which also showed a similar parallel transition displayed as a heatmap (online supplemental figure S2C); immune-poor tumors had significantly higher β Alt scores ([figure 2F](#)). To ascertain whether this relationship was generalizable, we analyzed breast cancer, which was not included in the immune archetype core specimens. The TCGA breast cancer specimens recapitulated a similar pattern of immune-rich to poor TeIS, paralleled by low to high β Alt (online supplemental figure S2D) and immune-poor tumors had significantly higher β Alt scores ([figure 2G](#)). Consistent with the correlation of high β Alt with immune-poor tumors, the expression of markers of cytotoxic T cells were uniformly negatively correlated with β Alt across cancer types (online supplemental figure S2E). Given the compelling evidence that dMMR, which has high predictive value in immunotherapy, gives rise to inflamed tumors,⁴¹ it is particularly surprising that genomically unstable²³ and radiosensitive²⁴ high β Alt cancers are immune-poor and IFN low.

High β Alt, immune-poor tumors can convert to immune-rich with treatment

It is well-established that loss of cell-intrinsic TGF β signaling in cancer cells can lead to increased TGF β activity, which was elegantly demonstrated in the KRAS lung model using tumor-specific clustered regularly interspaced short palindromic repeats (CRISPR) knockdown of *TGFR2* that resulted in lung tumors devoid of lymphocytes.⁴² Hence, loss of TGF β signaling can establish a highly immunosuppressive TME but how such tumors respond to ICB is unknown. To investigate this experimentally, we determined whether the association of β Alt with the immune context was evident in mouse tumors.

The TISMO database consists of 1500 mouse tumors covering 68 cell lines and 19 cancer types.³⁶ Unsupervised hierarchical clustering of untreated specimens using the TeIS signatures also resulted in a gradient from immune-rich to immune-poor accompanied by increasing β Alt scores (online supplemental figure 3A,B). 12 independently derived mTDT also exhibited this relationship (online supplemental figure 3C,D). Nearly half of the high β Alt mTDT were immune-poor (47%, 11/23). Family F mTDT clustered in the far right arm of the dendrogram with the highest β Alt score and lowest TeIS expression. The recapitulation in mouse models of the relationship between β Alt and immune context underscores its high conservation and provides the means to investigate how to target it therapeutically.

To this end, we used the high β Alt, low TeIS family F mTDT to investigate the response to TGF β i and an anti-PD-L1.²⁷ Because high β Alt cancer cells are unresponsive to TGF β , we hypothesized that TGF β i would be necessary to overcome immunosuppression caused by pronounced TGF β activity in the TME. To reveal the immunogenic potential of alt-EJ misrepair, we incorporated radiation therapy (RT) into the treatment strategy because it could increase antigen presentation since high β Alt tumors are radiation sensitive.⁴³ Mice bearing mTDT with an average volume of approximately 75 mm³ were randomized into treatment arms ([figure 3A](#)), consisting of 10 Gy single dose RT, anti-PD-L1 or TGF β i, dual combinations, or triple treatment. Monotherapy with anti-PD-L1 or TGF β i, as well as their combination, had little effect on survival. In contrast, triple treatment that included RT led to a significant increase in overall survival ([figure 3B](#)). The median survival time for monotherapy consisting of anti-PD-L1 or TGF β i and their dual combination was 8 days, which increased to 11 days with RT only. Dual therapy with RT plus anti-PD-L1 or TGF β i led to a median survival of 13 days, whereas triple treatment (combination plus RT) increased the median survival to 22 days.

Individual mice manifested two distinct patterns of early responses to treatment: tumors either grew exponentially after treatment or their growth was controlled during the first 7 days post-treatment (online supplemental figure 3E). This difference, early response versus growth, led us to classify mice across treatment groups as responders and non-responders at 7 days post-treatment ([figure 3C](#)). A similar classification was recently used to characterize the mouse tumor response to a bifunctional TGF β trap and anti-PD-1.⁴⁴ The difference in tumor growth rates of mice fashion classified in this was highly significantly ($p = 0.0023$; two-way ANOVA). The doubling time of tumors classified as responders ($n = 34$) was 9 days, and that of non-responders ($n = 24$) was 2.6 days (95% CI (2.2 to 3.1)). Tumor weight was also significantly lower in responders than in non-responders (Mann-Whitney test, $p = 0.007$, 95% CI (-0.42 to -1.76), [figure 3D](#)). Importantly, the overall survival of mice classified as responders was significantly longer than that of non-responders ([figure 3E](#)). The median survival was 8 days for untreated

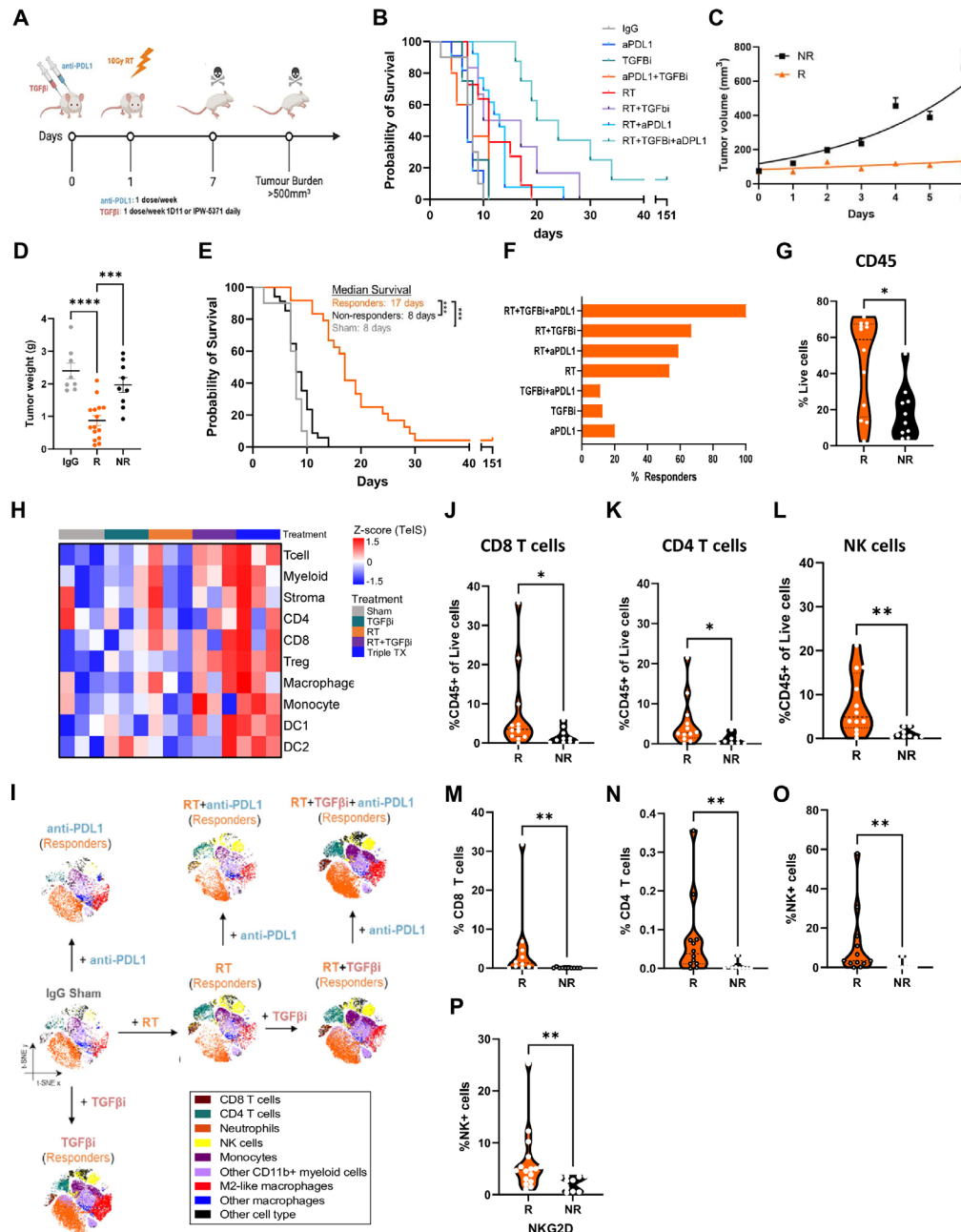


Figure 3 High β Alt, immune-poor mTDT respond to ICB by converting to immune-rich. (A) Experimental schematic of treatment schedule, primary endpoints and tissue collection. (B) Kaplan-Meier overall survival curves of mTDT treated with IgG isotype (gray, $n=8$), anti-PD-L1 (blue, $n=7$), TGF β i (green, $n=8$), anti-PD-L1+TGF β i (orange, $n=8$), 10Gy RT (red, $n=11$), RT+anti-PD-L1 (light blue, $n=13$), RT+TGF β i (purple, $n=6$) and RT+TGF β i+anti-PD-L1 (teal, $n=7$). $p<0.0001$ via log-rank test. (C) Mice classified as responders (R, orange, $n=34$) at 7 days post-treatment exhibit significantly decreased ($p=0.0023$; two-way ANOVA) growth trajectories (mean \pm SEM) compared with non-responders (NR, black, $n=24$). (D) Tumor weights (mean \pm SEM) of mice designated as R ($n=15$) were significantly less ($p<0.001$, one-way ANOVA) than those from mice treated with IgG isotype ($n=8$) or those designated as NR ($n=9$). (E) Kaplan-Meier overall survival of mice designated as R ($n=24$) were significantly longer ($p<0.001$, log-rank test) than mice designated as NR ($n=34$) or sham-treated ($n=10$). (F) Percentage of responders among treatment groups. (G) Percentage of live intratumoral CD45+ cells was significantly increased ($p<0.05$) in tumors designated as R ($n=12$) versus NR ($n=10$). (H) Heatmap showing TeIS-RNA deconvoluted immune cell populations of mTDT treated with IgG isotype, 10Gy RT, RT+TGF β i and RT+TGF β i+anti-PD-L1 ($n=3$ per group) 7 days post-treatment. (I) t-SNEs of tumor immune cell composition between R treated with same treatments in 3B. (J–L) CD45-normalized percentages of live intratumoral (J) CD8 T cells, (K) CD4 T cells and (L) NK cells, Proliferation, indicative of activation, marked by Ki67 in (M) Ki67+CD8 T cells, (N) Ki67+CD4 T cells, and (O) Ki67+NK cells was significantly increased in R. (P) Percentage of NK cell activation marker NKG2D positive cells was also significantly increased in R. Statistical significance is denoted as * $p<0.05$, ** $p<0.01$, *** $p<0.001$. ANOVA, analysis of variance; ICB, immune checkpoint blockade; IgG, immunoglobulin G; mTDT, mammary tumor-derived transplants; NK, natural killer; PD-L1, programmed death-ligand 1; RT, radiation; TeIS, tumor-educated immune signature; TGF β i, transforming growth factor-beta inhibition; t-SNE, t-distributed stochastic neighbor embedding.

mice or non-responders. In contrast, survival was more than doubled to 17 days in those classified as responders (log-rank, $p < 0.0001$).

The proportion of responders paralleled the survival outcomes with regard to therapy modality ($p = 0.0023$, two-way analysis of variance (ANOVA), [figure 3F](#)). Approximately 15–20% of the mice treated with either anti-PD-L1 or TGF β i as a monotherapy or dual combination were responders. The proportion of responders to RT tripled to 53%. In combination with RT, anti-PD-L1 therapy had little effect (58%), whereas RT and TGF β i increased the proportion of responders to 67%. All mice (9/9) were classified as responders following triple treatment with RT, anti-PD-L1, and TGF β i.

Uncoupling population responses from individual responses allowed the investigation of biological correlates of response to pinpoint early critical differences between responders and non-responders (online supplemental figure 3F). The frequency of CD45+leukocytes was significantly higher in tumors classified as responders than in those compared with non-responders (Mann-Whitney test, $p = 0.02$, [figure 3G](#)). Consistent with this, TeIS analysis of bulk RNA-sequencing data from treated tumors at 7 days showed increased intratumoral immune cell infiltration only when RT was combined with TGF β i, which was amplified with the addition of anti-PD-L1, essentially shifting the immune cold tumor to hot ([figure 3H](#)). This conclusion led to further functional investigation via multispectral flow cytometry. To identify and visualize immune cell populations, unsupervised analysis was performed using the dimensionality reduction algorithm t-SNE of responders across treatment groups ([figure 3I](#)). Plots from individual monotherapy treatments implicate RT and TGF β i as drivers of compositional changes in responders, whereas anti-PD-L1 had little effect. The frequency of tumor-infiltrating CD8+ and CD4+ T cells increased in responders ([figure 3J–K](#)). The most prominent cell type increased in responders was NK cells (Mann-Whitney test, $p = 0.003$, 95% CI (–1.22 to –13.3), [figure 3L](#)). Consistent with activation and clonal expansion, the proliferation of CD4+ and CD8+ T cells (Mann-Whitney test, $p = 0.003$; [figure 3M–N](#)) and NK cells (Mann-Whitney test, $p = 0.002$; [figure 3O](#)) was significantly increased in responders. In contrast, neither a number nor proliferation increase was evident in non-responders, regardless of treatment (online supplemental figure 3G,H). Moreover, increased immune reactivity within the tumor was paralleled by increased CD8+, CD4+ T cells, and NK cells in the blood of responders compared with non-responders (online supplemental figure 3I–K) whereas other blood immune cells did not change. The percentage of NK cells specifically increased in responders ([figure 3L](#)), which also exhibited, NKG2D, a marker of NK cell activation (Mann-Whitney test, $p < 0.001$; [figure 3P](#)). Hence, triple treatment converted a high β Alt, immune-poor tumor to immune-rich accompanied by significant activation of immune cells, and better tumor control.

NK cells mediate the response of β Alt high, immune-poor tumors to ICB therapy

NK cells were significantly increased in responders compared with non-responders or sham (ANOVA, $p < 0.008$; online supplemental figure 4A). The proportion of NK cells among responders ($n = 13$) nearly tripled from 2.8% in non-responders ($n = 10$) to 8% in responders. Moreover, activation, as indicated by Ki67 proliferation, markedly increased (online supplemental figure 4B). Indeed, treatment with TGF β i in combination with RT resulted in the most significant expansion and activation of NK cells compared with RT alone or RT combined with anti-PD-L1 ([figure 4A–C](#)). These findings were exemplified by the significant enrichment of NK cell activation signatures present in the transcriptomics from tumors treated with RT and TGF β i compared with controls ([figure 4D](#)).

We postulated that the increase in NK cells was the key to the recruitment of CD4 and CD8 T cells and the response to anti-PD-L1. High β Alt tumors are intrinsically deficient in DNA repair and recent studies have shown that blocking DNA repair in irradiated tumors can boost the response to ICB therapy by activating NK cells.⁴⁵ Moreover, TGF β broadly downregulates chemokine receptor expression necessary to recruit NK cells to the tumor and impairs NK cell function.⁴⁶

To test whether NK cells were critical, an NK depleting antibody was administered before RT alone or triple treatment with TGF β i and anti-PD-L1 ([figure 4E](#)). The efficacy of depletion was confirmed by the analysis of PBMC, in which both NK cells and proliferating NK cells were significantly decreased (online supplemental figure 4C,D). As in the prior study, infiltrating leukocytes increased significantly in tumors treated with the triple combination over RT alone, and was reduced to that of untreated tumors by NK depletion ([figure 4F](#)). Intratumoral NK cells, which were negative for a marker of innate lymphoid cell 1 (online supplemental figure 4E), were depleted in the triple treatment arm to negligible levels of the untreated tumors ([figure 4G](#)). NK depletion before triple treatment ($n = 12$) completely abrogated the 75% response rate of this combination (χ^2 , $p < 0.0001$) ([figure 4H](#)). The response to RT significantly increased (χ^2 , $p = 0.0004$) from 50% ($n = 11$) to 70% ($n = 11$).

NK cells are controlled through specific cell-surface receptors that can either stimulate or inhibit the activity of NK cells, and their combinatorial signaling dictates NK cell response and function.⁴⁷ The balance of activating to inhibitory signaling conditions in the NK cell-target synapse can be shifted by cytokines, particularly TGF β . We examined intracellular cytokine levels to understand better the mechanisms mediating the NK cell axis in high β Alt immune-poor tumors. Although CD8 T cells were not increased across treatments, interleukin-2 (IL-2)+CD8+ T cells were significantly increased in triple-treated tumors compared with untreated or irradiated tumors, which was abrogated by NK cell depletion ([figure 4I](#)). Similarly, cDC numbers were similar across treatments, but CXCL9+cDCs

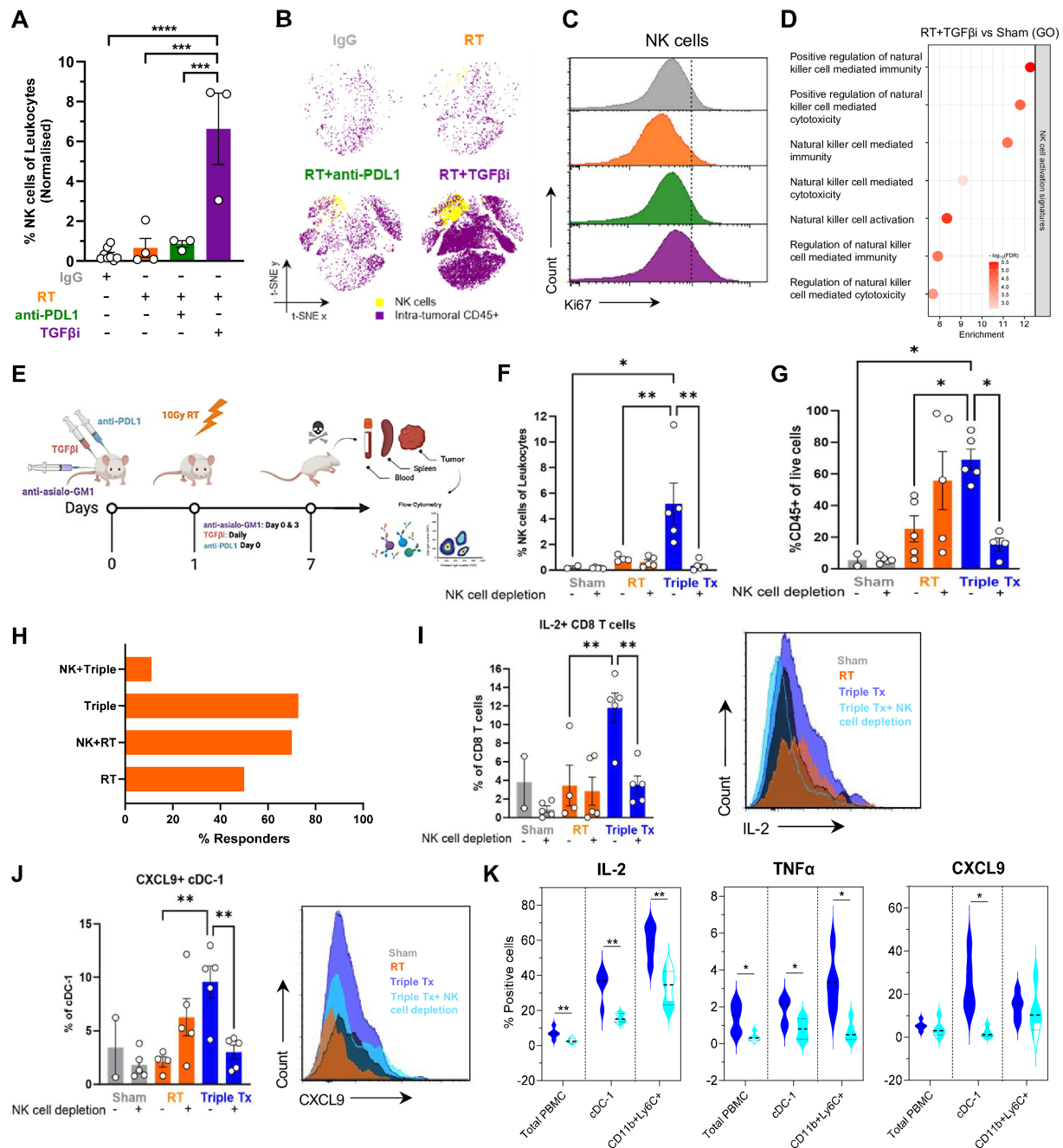


Figure 4 NK cells mediate the response of β Alt high, immune-poor tumors to ICB therapy. (A) CD45%-normalized percentage of NK cells in mTDT treated with RT+TGFβi (purple, n=3) were significantly increased compared with IgG (gray, n=8), RT (orange, n=4), RT+anti-PD-L1 (green, n=3). One-way ANOVA. (B) t-SNEs depicting tumor NK cells (yellow) and CD45+ (purple) cells in mTDT treated as above. Depicted cell numbers across treatments have been normalized for CD45+infiltration. (C) Representative fluorescence histograms of Ki67 in tumor-infiltrating NK cells treated as in A. (D) Gene ontology enrichment for NK cell activation signatures in mice treated with RT+TGFβi compared with sham-treated 7 days post-treatment. (E) NK cell depletion experimental schematic of treatment schedule, primary endpoint, and tissue collection. Percentages of live intratumoral (F) CD45+ cells and (G) %CD45-normalized NK cells. (H) Percentage of responders between treatment groups. Percentages of live intratumoral (I) %CD8 T cells IL-2+ and (J) %cDC-1 CXCL9+ cells between F mTDT treated with IgG isotype without (n=2) or with NK cell depletion (n=5) or with (n=5) NK cell depletion, representative fluorescence histograms (right). (K) Percentage of circulating IL-2, TNFα, and CXCL9 in total PBMC (left), cDC-1 (middle) and CD11b+Ly6C+ cells (right) increased in mTDT following triple TX (blue) versus triple TX+NK depletion (light blue). Unpaired t-tests. Data are depicted as mean±SEM; each point represents a mouse, and one-way ANOVA p values are represented as follows: *p<0.05, **p<0.01, ***p<0.001. ANOVA, analysis of variance; cDC, classical dendritic cell; FDR, false discovery rate; GO, Gene Ontology; ICB, immune checkpoint blockade; IgG, immunoglobulin G; IL-2, interleukin-2; mTDT, mammary tumor-derived transplants; NK, natural killer; PBMC, peripheral blood mononuclear cell; PD-L1, programmed death-ligand 1; RT, radiation; TGFβi, transforming growth factor-beta inhibition; t-SNE, t-distributed stochastic neighbor embedding.

were significantly increased only in tumors following triple combination treatment (figure 4J). We hypothesize that the crosstalk of activated NK cells and cDC maintains a positive feedback loop for the chemotactic recruitment of immune cells through CXCL9 release. Levels of the cytokines IL-2, TNF α , and CXCL9 in circulating immune cells, which were increased by triple treatment, were also NK cell-dependent (figure 4K). Thus, the unique TME of high β Alt tumors can be primed for checkpoint blockade by promoting an NK cell-dependent response, detectable both in the tumor and circulation.

High β Alt, immune-poor tumors convert to immune-rich that respond to ICB

Restoration of NK cell function in cancer has been hypothesized to activate tumor immunity.⁴⁷ To determine the generalizability of the mechanism, we used the TISMO database, which comprises data from syngeneic mouse tumors treated with ICB. We identified two widely used tumor models, melanoma B16 and colorectal CT26 as high β Alt and immune-poor, as measured by TeIS, at baseline (figure 5A and C). Notably, response to an ICB shifted most of the tumors to an immune-rich phenotype ($p < 0.0001$, χ^2 test). Moreover, the gene ontology signatures of NK activation were significantly enriched in responders (figure 5B and D).

To ascertain whether this mechanism is evident in human cancers, we analyzed the GSE91061 data set in which paired biopsies from patients with advanced melanoma ($n=43$) were obtained before and after treatment with anti-PD-1 (nivolumab).³³ Nine patients were classified as responders to anti-PD-1 therapy and 34 as non-responders. As with IMvigor210, TGF β and alt-EJ signatures were anticorrelated, although there was no significant difference in the mean β Alt of complete and partial responders compared with stable or progressive disease pretreatment in this small group. Based on TeIS unsupervised clustering, there was however a marked association between high β Alt levels and immune-poor TME (online supplemental figure 4F). We compared the pretreatment and on-treatment TeIS signatures of responders for whom transcriptomics was available ($n=9$). Two responders, classified as high β Alt and immune-poor pretreatment, moved to immune-rich in the on-treatment biopsy (online supplemental figure 4G). None of the patients classified as immune-rich moved on treatment, regardless of the β Alt score. Genes associated with NK activation also increased in patients with high β Alt paired biopsy melanoma in response to anti-PD-1 therapy (online supplemental figure 4H). Although the sample size is small, these human data support the experimental studies whereby NK cell-mediated lymphocyte recruitment facilitates ICB response in high β Alt, immune-poor tumors. We suggest that β Alt and TeIS provide the means to prospectively identify a previously unrecognized subset of immune-poor patients in whom TGF β i reverses resistance to ICB (figure 5E).

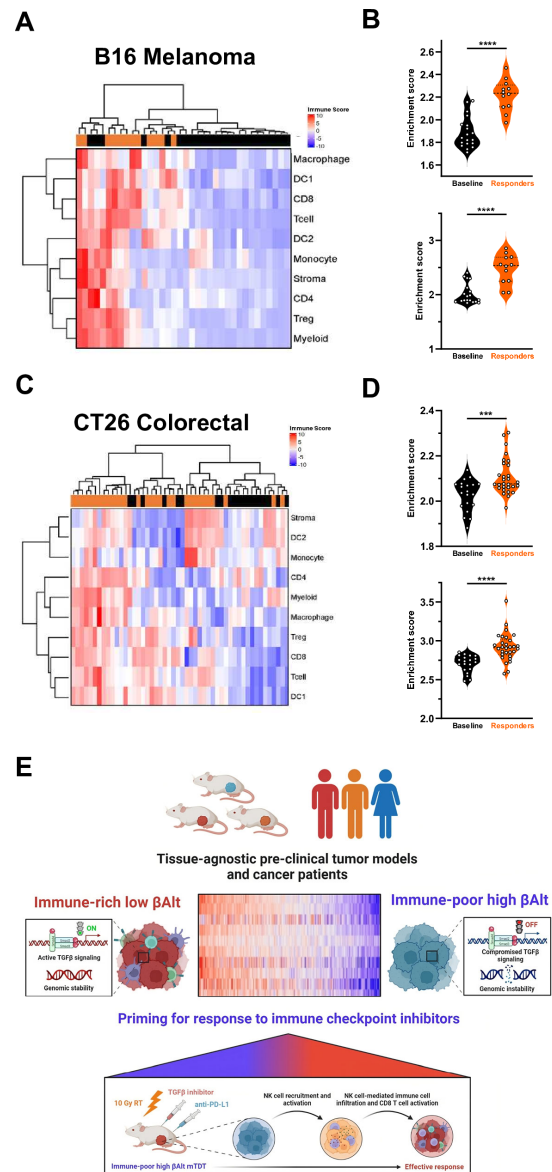


Figure 5 High β Alt, immune-poor tumors convert to immune-rich on response to ICB. (A) Unsupervised hierarchical TeIS clustering of B16 melanoma model at baseline (black, $n=19$) versus responsive to ICB treatment (orange, $n=12$). (B) Gene ontology signatures of NK activation (top) and NK mediated immunity (bottom) of B16 baseline versus response to ICB treatment. Unpaired t-test. (C) Unsupervised hierarchical TeIS clustering of CT26 melanoma model at baseline (black, $n=20$) versus responsive to ICB treatment (orange, $n=30$). (D) Gene ontology signatures of NK activation (top) and NK mediated immunity (bottom) of CT26 baseline versus response to dual ICB treatment. Unpaired t-test. (E) Graphical summary depicting low β Alt tumors, which have active TGF β signaling and genomic stability, are immune-rich, while high β Alt tumors that have low TGF β signaling and genomic instability are immune-poor. Both human data and experimental studies indicate that NK cell-mediated lymphocyte recruitment facilitates ICB response in high β Alt, immune-poor tumors. ICB, immune checkpoint blockade; mTDT, mammary tumor-derived transplants; NK, natural killer; PD-L1, programmed death-ligand 1; RT, radiation; TeIS, tumor-educated immune signature; TGF β , transforming growth factor-beta.

DISCUSSION

Predicting patient response to immunotherapy is complicated by an incomplete understanding of the immune context,⁴⁸ the diversity of the systemic immune environment,⁴⁹ and the complexity of the drivers of cancer immunity.⁵⁰ Here we show that patients with high β Alt tumors, in which both TGF β signaling and DNA repair are compromised, are responsive to ICB treatment. We hypothesized that loss of TGF β signaling feedback resulted in compensatory TGF β generation that masks the immunogenic potential of alt-EJ misrepair. Preclinical modeling identified a therapeutic combination of TGF β i and RT was able to instigate the conversion of immune-poor to immune-rich, evidenced by lymphocytic infiltration. Analysis of high β Alt mouse tumors and clinical trial data showed that NK cell activation was instrumental in converting immune-poor tumors to immune-rich. The identification of ICB-responsive cold cancers in which intrinsic loss of TGF β signaling generates TGF β rich, immunosuppressive TME suggests that patients selected using a biomarker consisting of combined TGF β , DNA repair, and immune context signatures could benefit clinical trials of combination treatment with TGF β inhibitors and immunotherapy.

The precise cellular and molecular pathways that lead some patients to respond, while others do not, remain largely undefined because the complex biology of the immune microenvironment is incompletely understood.⁵⁰ Although lymphocytic infiltration is generally associated with response, there is a significant need for a biomarker to identify some patients with poorly infiltrated tumors who still benefit from ICB. In contrast to the inflamed phenotype of dMMR,^{13 51} the genomic and phenotypic consequences of compromised TGF β signaling and error-prone alt-EJ repair result in an immune-poor tumor lacking lymphocytes and IFN signaling. The paradoxical consequence of high β Alt is an immunosuppressive TME, underscoring the tightly coupled intrinsic and extrinsic actions of TGF β . Whereas the DNA misrepair from dMMR elicits type-I IFN that recruits lymphocytes, the high levels of misrepair from alt-EJ are overridden by an established TGF β -rich TME. We speculate that cancer cells that lose TGF β signaling competency early in carcinogenesis increase TGF β activity that establishes an immunosuppressive TME lacking lymphocytes. It may be that loss of TGF β also compromises innate DNA sensing mechanisms, thereby indirectly suppressing IFN, further endorsing the immune cold TME, but the mechanism is not yet known.

The clinical success of cancer immunotherapy is predicated on disrupting the equilibrium established between the patient's cancer and their immune system.⁵² A deeper understanding of the diversity of the systemic immune environment across human malignancies is critical for improving immunotherapy treatment strategies. Our analysis was aided by the immune archetype paradigm based on an immune profiling initiative that conducted a holistic survey across cancers.²⁹ Our analyses and

preclinical data show that high β Alt, immune-poor mouse and human tumors represent a category of malignancies that can be shifted from immune-poor to immune-rich by different treatments and thus have the potential to benefit from ICB. We found that RT and TGF β i was able to recruit and activate T cells via NK cells in the high β Alt, immune-poor mTDT. The widely used high β Alt and immune-poor B16 melanoma and CT26 colorectal models also shift to immune-rich in response to ICB. Although there are limited data from humans, a small, paired biopsy study reported by Riaz *et al*³³ shows that high β Alt, immune-poor melanoma cancers can shift to immune-rich in response to ICB therapy.

We found that TGF β i leads to the activation of NK cells that are well known to be suppressed by TGF β ,^{53–55} which provide an actionable route by which immune-poor, high β Alt tumors can respond to ICB. In contrast to the prominent role of CD8 T cells in the ICB response of immune-infiltrated tumors, we found that NK depletion completely abrogated both lymphocytic infiltration and the ICB response in high β Alt and immune-poor mTDT. Moreover, NK cell activation signatures increased on treatment response in high β Alt, immune-poor F mTDT, B16, and CT26 mouse tumors, and patients with melanoma. NK cells correlate with better overall survival in various solid cancers, including gastric, breast, and renal cell carcinoma, and increased response to checkpoint blockade immunotherapy in melanoma.^{56 57} Immunosuppressive TGF β broadly downregulates chemokine receptor expression necessary to recruit NK cells to the TME and impairs NK cell function by limiting NK cell antibody-dependent cellular cytotoxicity.⁴⁶ Although the mechanisms mediating the suppression of the NK cell axis are not yet fully understood, the data reported here highlight consideration of NK cell-mediated contributions to lymphocyte recruitment that convert ICB resistant tumors to ICB responsive.

Because the immune system is a distributed organ that has a regulated repertoire of mechanisms to suppress cancer, research on cancer immunity is moving away from tissue-of-origin specificity toward tissue-agnostic ecosystems and processes.^{58 59} The more nuanced classification of cancer by immune archetypes is a significant advancement that will enhance patient outcomes by enabling the selection of optimal therapeutic strategies. Although how cancer cells determine the granular immune TME is still unclear,⁶⁰ a high β Alt signature describes a TGF β incompetent tumor cells embedded in a TME in which TGF β is the major determinant of immunosuppression.

The main limitation of our study stems from the retrospective analysis of clinical trial data, whereas the prospective application of β Alt to stratify patients for optimal treatment would provide the strongest evidence of clinical utility. We assessed immune context by one classification scheme, immune archetypes, but there are many immune signatures that may provide additional information. Also, there is a growing appreciation of spatial

patterning as an important determinant of response to therapy that could add to our assessment of the high β Alt tumor phenotype. In experimental modeling, the high β Alt tumor was derived from the breast, whereas the ICB trial data were bladder cancer or melanoma; there may be tissue-specific features that modify ICB response in a manner not captured by our analysis. Indeed breast cancer is one of the least ICB-responsive solid cancers.⁶¹ Our preclinical modeling combined radiotherapy and ICB, yet most trials of such combinations have not shown significant benefit at the population level.⁶² We postulate that RT-induced cell death reveals the immunogenic potential of DNA misrepaired by alt-EJ, but whether this will be borne out in humans and its potential context-specificity remains to be seen.

To date, no TGF β inhibitors have been approved in cancer therapy, despite strong preclinical evidence that TGF β activity drives malignancy and immunosuppression. We suggest that our studies provide the means to prospectively identify a previously unrecognized subset of immune-poor patients in whom TGF β i reverses resistance to ICB. Further validation of the β Alt signature to predict patient outcomes requires analysis of additional data sets, ideally ones in which paired biopsies and transcriptomics are available pre-ICB and post or during ICB. Substantial opportunity exists to use β Alt and TeIS scores to inform TGF β inhibitor trials that are underway in combinations with ICB for multiple indications, including therapeutic avenues to activate NK cells and NK cell therapies that might be particularly effective in high β Alt tumors.

Author affiliations

¹Department of Radiation Oncology, University of California San Francisco, San Francisco, California, USA

²Oncology Biomarker Development, Genentech, South San Francisco, California, USA

³Division of Oral Epidemiology and Division of Biostatistics, University of California San Francisco, San Francisco, California, USA

⁴Depts of Otolaryngology-Head and Neck Surgery and of Microbiology and Immunology, University of California San Francisco, San Francisco, California, USA

⁵Department of Pathology, University of California San Francisco, San Francisco, California, USA

X Matthew Spitzer @SpitzerLab

Acknowledgements The authors would like to thank Drs David Nyguen and Hang Chang for data analysis, Trevor Jones and Colin Foster, and Hui Zhang in the Barcellos-Hoff lab, and Bushra Samad of the University of California, San Francisco Data Science Co-Lab for their support of this research. The results presented here are partly based on the analysis of data generated by The Cancer Genome Atlas (TCGA) Research Network (<https://www.cancer.gov/tcga>), and we would like to express our gratitude to the TCGA consortia and their coordinators for the data provision and clinical information used in this study.

Contributors Conceptualization: MHB-H, JM. Methodology: MHB-H, JM. Statistician: AAL. Investigation: JM, JG, IG, KY, AC. Visualization: MHB-H, JM, JG. Funding acquisition: MHB-H, MS. Project administration: MHB-H. Guarantor: MHB-H. Writing—original draft: MHB-H, JM. Writing—review and editing: All.

Funding Genentech imCORE network project UCS-3 (MHBH) Genentech imCORE network project UCS-7 (MHS) Genentech imCORE network project UCS-12 (MHBH) National Institutes of Health grant R01CA190980 (MHBH) National Institutes of Health grant R01CA239235 (MHBH) National Institutes of Health grant R01CA190980S1 (JM) National Institutes of Health grant T32CA108462 (JM) The CyTOF instrument was procured with the support of the National Institutes of Health

(grant S10 OD018040). Tissue processing and immunostaining were performed using the Helen Diller Family Comprehensive Cancer Center Pathology Shared Resource, supported by the National Cancer Institute of the National Institutes of Health under Award Number P30CA082103. IPW was provided under a material transfer agreement with Innovations Pathway, Inc.

Competing interests MHB-H reports grants and non-financial support from Genentech, personal fees and non-financial support from Innovation Pathways, personal fees from Scholar Rock and Vericte, and non-financial support from Bicara during the conduct of the study. MHB-H, IG and JM filed a provisional patent 63/629977 on March 12, 2024. KY is an employee of Genentech. MS is a founder, shareholder, and board member of Teiko.bio, has received a speaking honorarium from Fluidigm, has been a paid consultant for Five Prime, Ono, January, Earli, Astellas, and Indaptus, and has received research funding from Roche/Genentech, Pfizer, Valitor, and Bristol Myers Squibb.

Patient consent for publication Not applicable.

Ethics approval Not applicable.

Provenance and peer review Not commissioned; externally peer reviewed.

Data availability statement Data are available in a public, open access repository. Code Availability: β AltW code: <https://github.com/pujana-lab/Under-review-article> Data Availability: The public availability of the transcriptomic data generated in this study is pending.

Supplemental material This content has been supplied by the author(s). It has not been vetted by BMJ Publishing Group Limited (BMJ) and may not have been peer-reviewed. Any opinions or recommendations discussed are solely those of the author(s) and are not endorsed by BMJ. BMJ disclaims all liability and responsibility arising from any reliance placed on the content. Where the content includes any translated material, BMJ does not warrant the accuracy and reliability of the translations (including but not limited to local regulations, clinical guidelines, terminology, drug names and drug dosages), and is not responsible for any error and/or omissions arising from translation and adaptation or otherwise.

Open access This is an open access article distributed in accordance with the Creative Commons Attribution Non Commercial (CC BY-NC 4.0) license, which permits others to distribute, remix, adapt, build upon this work non-commercially, and license their derivative works on different terms, provided the original work is properly cited, appropriate credit is given, any changes made indicated, and the use is non-commercial. See <http://creativecommons.org/licenses/by-nc/4.0/>.

ORCID iD

Mary Helen Barcellos-Hoff <http://orcid.org/0000-0002-5994-9558>

REFERENCES

- Sharma P, Allison JP. The future of immune checkpoint therapy. *Science* 2015;348:56–61.
- Topalian SL, Taube JM, Anders RA, *et al.* Mechanism-driven biomarkers to guide immune checkpoint blockade in cancer therapy. *Nat Rev Cancer* 2016;16:275–87.
- Yarchoan M, Hopkins A, Jaffee EM. Tumor Mutational Burden and Response Rate to PD-1 Inhibition. *N Engl J Med* 2017;377:2500–1.
- Thomas A, Routh ED, Pullikuth A, *et al.* Tumor mutational burden is a determinant of immune-mediated survival in breast cancer. *Oncoimmunology* 2018;7:e1490854.
- Chan TA, Yarchoan M, Jaffee E, *et al.* Development of tumor mutation burden as an immunotherapy biomarker: utility for the oncology clinic. *Ann Oncol* 2019;30:44–56.
- Anagnostou V, Bardelli A, Chan TA, *et al.* The status of tumor mutational burden and immunotherapy. *Nat Cancer* 2022;3:652–6.
- Hegde PS, Karanikas V, Evers S. The Where, the When, and the How of Immune Monitoring for Cancer Immunotherapies in the Era of Checkpoint Inhibition. *Clin Cancer Res* 2016;22:1865–74.
- Bagaev A, Kotlov N, Nomie K, *et al.* Conserved pan-cancer microenvironment subtypes predict response to immunotherapy. *Cancer Cell* 2021;39:845–65.
- Galon J, Bruni D. Approaches to treat immune hot, altered and cold tumours with combination immunotherapies. *Nat Rev Drug Discov* 2019;18:197–218.
- Mariathasan S, Turley SJ, Nickles D, *et al.* TGF β attenuates tumour response to PD-L1 blockade by contributing to exclusion of T cells. *Nature New Biol* 2018;554:544–8.
- Shen J, Choi Y-L, Lee T, *et al.* Inflamed immune phenotype predicts favorable clinical outcomes of immune checkpoint inhibitor

- therapy across multiple cancer types. *J Immunother Cancer* 2024;12:e008339.
- 12 Roller A, Davydov II, Schwalie PC, *et al.* Tumor-agnostic transcriptome-based classifier identifies spatial infiltration patterns of CD8+T cells in the tumor microenvironment and predicts clinical outcome in early-phase and late-phase clinical trials. *J Immunother Cancer* 2024;12:e008185.
 - 13 Le DT, Durham JN, Smith KN, *et al.* Mismatch repair deficiency predicts response of solid tumors to PD-1 blockade. *Science* 2017;357:409–13.
 - 14 Chalabi M, Fanchi LF, Dijkstra KK, *et al.* Neoadjuvant immunotherapy leads to pathological responses in MMR-proficient and MMR-deficient early-stage colon cancers. *Nat Med* 2020;26:566–76.
 - 15 Formenti SC, Demaria S. Combining radiotherapy and cancer immunotherapy: a paradigm shift. *J Natl Cancer Inst* 2013;105:256–65.
 - 16 Lake RA, Robinson BWS. Immunotherapy and chemotherapy--a practical partnership. *Nat Rev Cancer* 2005;5:397–405.
 - 17 Lu C, Guan J, Lu S, *et al.* DNA Sensing in Mismatch Repair-Deficient Tumor Cells Is Essential for Anti-tumor Immunity. *Cancer Cell* 2021;39:96–108.
 - 18 Derynck R, Turley SJ, Akhurst RJ. TGF β biology in cancer progression and immunotherapy. *Nat Rev Clin Oncol* 2021;18:9–34.
 - 19 Nixon BG, Gao S, Wang X, *et al.* TGF β control of immune responses in cancer: a holistic immuno-oncology perspective. *Nat Rev Immunol* 2023;23:346–62.
 - 20 Barcellos-Hoff MH. The radiobiology of TGF β . *Semin Cancer Biol* 2022;86:857–67.
 - 21 Liu Q, Lopez K, Murnane J, *et al.* Misrepair in Context: TGF β Regulation of DNA Repair. *Front Oncol* 2019;9:799.
 - 22 Liu Q, Chen G, Moore J, *et al.* Exploiting Canonical TGF β Signaling in Cancer Treatment. *Mol Cancer Ther* 2022;21:16–24.
 - 23 Liu Q, Palomero L, Moore J, *et al.* Loss of TGF β signaling increases alternative end-joining DNA repair that sensitizes to genotoxic therapies across cancer types. *Sci Transl Med* 2021;13:eabc4465.
 - 24 Guix I, Liu Q, Pujana MA, *et al.* Validation of Anticorrelated TGF β Signaling and Alternative End-Joining DNA Repair Signatures that Predict Response to Genotoxic Cancer Therapy. *Clin Cancer Res* 2022;28:1372–82.
 - 25 Kornepati AVR, Rogers CM, Sung P, *et al.* The complementarity of DDR, nucleic acids and anti-tumour immunity. *Nature New Biol* 2023;619:475–86.
 - 26 Ceccaldi R, Rondinelli B, D'Andrea AD. Repair Pathway Choices and Consequences at the Double-Strand Break. *Trends Cell Biol* 2016;26:52–64.
 - 27 Moore J, Ma L, Lazar AA, *et al.* Mammary Tumor-Derived Transplants as Breast Cancer Models to Evaluate Tumor-Immune Interactions and Therapeutic Responses. *Cancer Res* 2022;82:365–76.
 - 28 Gu Z, Eils R, Schlesner M. Complex heatmaps reveal patterns and correlations in multidimensional genomic data. *Bioinformatics* 2016;32:2847–9.
 - 29 Combes AJ, Samad B, Tsui J, *et al.* Discovering dominant tumor immune archetypes in a pan-cancer census. *Cell* 2022;185:184–203.
 - 30 Kandoth C, McLellan MD, Vandin F, *et al.* Mutational landscape and significance across 12 major cancer types. *Nature New Biol* 2013;502:333–9.
 - 31 Banchereau R, Leng N, Zill O, *et al.* Molecular determinants of response to PD-L1 blockade across tumor types. *Nat Commun* 2021;12:3969.
 - 32 Hugo W, Zaretsky JM, Sun L, *et al.* Genomic and Transcriptomic Features of Response to Anti-PD-1 Therapy in Metastatic Melanoma. *Cell* 2016;165:35–44.
 - 33 Riaz N, Havel JJ, Makarov V, *et al.* Tumor and Microenvironment Evolution during Immunotherapy with Nivolumab. *Cell* 2017;171:934–49.
 - 34 Kim D, Pertea G, Trapnell C, *et al.* TopHat2: accurate alignment of transcriptomes in the presence of insertions, deletions and gene fusions. *Genome Biol* 2013;14:R36.
 - 35 Trapnell C, Pachter L, Salzberg SL. TopHat: discovering splice junctions with RNA-Seq. *Bioinformatics* 2009;25:1105–11.
 - 36 Zeng Z, Wong CJ, Yang L, *et al.* TISMO: syngeneic mouse tumor database to model tumor immunity and immunotherapy response. *Nucleic Acids Res* 2022;50:D1391–7.
 - 37 Rosenberg JE, Hoffman-Censits J, Powles T, *et al.* Atezolizumab in patients with locally advanced and metastatic urothelial carcinoma who have progressed following treatment with platinum-based chemotherapy: a single-arm, multicentre, phase 2 trial. *The Lancet* 2016;387:1909–20.
 - 38 Balar AV, Galsky MD, Rosenberg JE, *et al.* Atezolizumab as first-line treatment in cisplatin-ineligible patients with locally advanced and metastatic urothelial carcinoma: a single-arm, multicentre, phase 2 trial. *Lancet* 2017;389:67–76.
 - 39 Bergmann CB, Beckmann N, Salyer CE, *et al.* Potential Targets to Mitigate Trauma- or Sepsis-Induced Immune Suppression. *Front Immunol* 2021;12:622601.
 - 40 Baysoy A, Bai Z, Satija R, *et al.* The technological landscape and applications of single-cell multi-omics. *Nat Rev Mol Cell Biol* 2023;24:695–713.
 - 41 Alouani E, Rousseau B, Andre T, *et al.* Immunotherapy advances in cancers with mismatch repair or proofreading deficiencies. *Nat Cancer* 2022;3:1414–7.
 - 42 Dhainaut M, Rose SA, Akturk G, *et al.* Spatial CRISPR genomics identifies regulators of the tumor microenvironment. *Cell* 2022;185:1223–39.
 - 43 Formenti SC, Demaria S. Radiation therapy to convert the tumor into an in situ vaccine. *Int J Radiat Oncol Biol Phys* 2012;84:879–80.
 - 44 Strait AA, Woolaver RA, Hall SC, *et al.* Distinct immune microenvironment profiles of therapeutic responders emerge in combined TGF β /PD-L1 blockade-treated squamous cell carcinoma. *Commun Biol* 2021;4:1005.
 - 45 Patin EC, Dillon MT, Nenclares P, *et al.* Harnessing radiotherapy-induced NK-cell activity by combining DNA damage-response inhibition and immune checkpoint blockade. *J Immunother Cancer* 2022;10:e004306.
 - 46 Lazarova M, Steinle A. Impairment of NKG2D-Mediated Tumor Immunity by TGF- β . *Front Immunol* 2019;10:2689.
 - 47 Cerwenka A, Lanier LL. Natural killer cell memory in infection, inflammation and cancer. *Nat Rev Immunol* 2016;16:112–23.
 - 48 Chen DS, Mellman I. Oncology meets immunology: the cancer-immunity cycle. *Immunity* 2013;39:1–10.
 - 49 Hiam-Galvez KJ, Allen BM, Spitzer MH. Systemic immunity in cancer. *Nat Rev Cancer* 2021;21:345–59.
 - 50 Hegde PS, Chen DS. Top 10 Challenges in Cancer Immunotherapy. *Immunity* 2020;52:17–35.
 - 51 Llosa NJ, Cruise M, Tam A, *et al.* The vigorous immune microenvironment of microsatellite instable colon cancer is balanced by multiple counter-inhibitory checkpoints. *Cancer Discov* 2015;5:43–51.
 - 52 Mittal D, Gubin MM, Schreiber RD, *et al.* New insights into cancer immunoediting and its three component phases--elimination, equilibrium and escape. *Curr Opin Immunol* 2014;27:16–25.
 - 53 Regis S, Dondero A, Caliendo F, *et al.* NK Cell Function Regulation by TGF- β -Induced Epigenetic Mechanisms. *Front Immunol* 2020;11:311.
 - 54 Powell AB, Yadavilli S, Saunders D, *et al.* Medulloblastoma rendered susceptible to NK-cell attack by TGF β neutralization. *J Transl Med* 2019;17:321.
 - 55 Wilson EB, El-Jawhari JJ, Neilson AL, *et al.* Human tumour immune evasion via TGF- β blocks NK cell activation but not survival allowing therapeutic restoration of anti-tumour activity. *PLoS ONE* 2011;6:e22842.
 - 56 Denkert C, von Minckwitz G, Darb-Esfahani S, *et al.* Tumour-infiltrating lymphocytes and prognosis in different subtypes of breast cancer: a pooled analysis of 3771 patients treated with neoadjuvant therapy. *Lancet Oncol* 2018;19:40–50.
 - 57 Huntington ND, Cursons J, Rautela J. The cancer-natural killer cell immunity cycle. *Nat Rev Cancer* 2020;20:437–54.
 - 58 Keidar Haran T, Keren L. From genes to modules, from cells to ecosystems. *Mol Syst Biol* 2022;18:e10726.
 - 59 Hoadley KA, Yau C, Hinoue T, *et al.* Cell-of-Origin Patterns Dominate the Molecular Classification of 10,000 Tumors from 33 Types of Cancer. *Cell* 2018;173:291–304.
 - 60 Chen DS, Mellman I. Elements of cancer immunity and the cancer-immune set point. *Nature New Biol* 2017;541:321–30.
 - 61 Garufi G, Carbognin L, Schettini F, *et al.* Updated Neoadjuvant Treatment Landscape for Early Triple Negative Breast Cancer: Immunotherapy, Potential Predictive Biomarkers, and Novel Agents. *Cancers (Basel)* 2022;14:4064.
 - 62 Pointer KB, Pitroda SP, Weichselbaum RR. Radiotherapy and immunotherapy: open questions and future strategies. *Trends Cancer* 2022;8:9–20.